iMRI 2023;27(1);21-31
https://doi.org/10.13104/imri.2022.1001
eISSN 2384-1109

Original Article

Received: April 11, 2022
Revised: August 25, 2022
Accepted: September 16, 2022

Correspondence
Eun-Suk Cha, MD, PhD
Department of Radiology,
Ewha Womans University
School of Medicine,
1071 Anyangcheon-ro,
Yangcheon-gu, Seoul 07985, Korea.
E-mail: escha@ewha.ac.kr

Response Evaluation to Neoadjuvant Chemotherapy in Breast Cancer Patients: Sequential Dynamic Contrast-Enhanced MRI Using Computer-Aided Detection

In Hye Chae[1], Eun-Suk Cha[2], Jee Eun Lee[2], Jin Chung[2], Jeoung Hyun Kim[2], Sun Hee Sung[3], and Mira Han[4]

[1]Department of Health Promotion, Yonsei University Health System, Severance Health Check-Up, Seoul, Korea
[2]Department of Radiology, Ewha Womans University School of Medicine, Seoul, Korea
[3]Department of Pathology, Ewha Womans University Mokdong Hospital, Ewha Womans University School of Medicine, Seoul, Korea
[4]Biostatistics Collaboration Team, National Cancer Center, Goyang, Korea

Purpose: We evaluated whether there is an association between sequential changes in kinetic profiles by computer-aided detection (CAD) during neoadjuvant chemotherapy (NAC) and pathologic complete response (pCR) and residual cancer burden (RCB) in dynamic contrast-enhanced MRI (DCE-MRI) of patients with invasive breast cancer.
Materials and Methods: This retrospective study involved 51 patients (median age, 48 years; range, 33–60 years) who underwent pre-, interim-, and post-NAC DCE-MRIs at 3 T. The tumor size and CAD-generated kinetic profiles (peak enhancement and delayed enhancement [persistent, plateau, and washout] components) were measured. Percentage changes in pre- and interim-NAC (ΔMRI value1) and pre- and post-NAC (ΔMRI value2) were compared between pCR and non-pCR cases, and according to RCB. Receiver operating characteristic curve analysis was performed to evaluate the association between pCR and MRI parameters (including CAD-generated kinetic profiles).
Results: The pCR rate was 19.6% (10/51). There were statistically significant differences in Δtumor size2 ($p < 0.01$), Δpeak enhancement2 ($p = 0.01$), Δpersistent2 ($p = 0.01$), Δplateau2 ($p = 0.02$), and Δwashout2 ($p = 0.03$) between pCR and non-pCR. ΔTumor size2 provided very good diagnostic accuracy for pCR (cut-off, -90%; area under the curve, 0.88). There were differences in Δtumor size2, Δpeak enhancement2, Δplateau2, and Δwashout2 between RCB classes ($p < 0.01$).
Conclusion: DCE-MRI using CAD has the potential for predicting pCR and RCB classes.

Keywords: Breast neoplasm; Neoadjuvant therapy; Magnetic resonance imaging; Computer-aided

INTRODUCTION

Neoadjuvant chemotherapy (NAC) is a standard treatment option for patients with locally advanced breast cancer. Approximately 30% of breast cancer patients receiving NAC show a pathologic complete response (pCR) [1]. Those who achieve pCR after NAC have a significantly higher disease-free survival and overall survival rate than those with residual disease (RD) [1-3]. On the other hand, the residual cancer burden (RCB) is a reporting system used to define pathologic response and it specifically focuses on RD. The RCB is a significant predictor of distant relapse-free survival [3].

Since the achievement of pCR after NAC is a predictor for superior long-term effects of systemic treatment and outcome, many studies have explored tumor responses to NAC using various imaging modalities [4]. Among them, dynamic contrast-enhanced MRI (DCE-MRI) is a reliable technique for assessing treatment response and estimating RD [4]. A meta-analysis of 44 studies reported that DCE-MRI showed high sensitivity (83%–87%) and heterogeneous specificity (54%–83%) in detection of residual cancer after NAC [5].

Computer-aided detection (CAD) for DCE-MRI receives the kinetic data of the whole contrast-enhanced lesions and calculates the kinetic profiles, and generates color maps and graphs. Several studies have used CAD to assess treatment response [6-8] and predict the outcomes in patients with breast cancer receiving NAC [9]. However, these studies primarily analyzed MRI data before and after NAC. To the best of our knowledge, there are no studies that have evaluated changes in the kinetic profiles of MRI data before, interim, and after NAC and investigated their association tumor response and RCB using CAD. Moreover, there is no study that has explored changes in CAD-generated kinetic profiles during NAC in different breast cancer subtypes.

Thus, the aim of the current study was to retrospectively evaluate whether the sequential changes in CAD-generated kinetic profiles by a DCE-MRI during NAC are associated with pCR and RCB in breast cancer patients. In addition, we investigated the characteristics of DCE-MRI parameters according to breast cancer subtypes.

MATERIALS AND METHODS

Study Population

This retrospective study was approved by the Institutional Review Board (IRB) of Ewha Womans University Mokdong Hospital (Approval number 2017-11-039), and informed consent was waived. A total of 93 patients with invasive breast cancer who underwent NAC in our institution between September 2015 and August 2017 were initially included in our study. Among the 93, 42 patients were excluded for the following reasons: 1 patient did not undergo interim MRI, 20 patients underwent relatively short NAC cycles (3 or 4 times), 12 patients did not have pre-NAC CAD data because the initial MRIs were taken at another hospital, 7 patients did not undergo surgery, and 2 patients did not undergo MRI scanning. Finally, 153 datasets of 51 eligible patients (median age: 48 years [range, 33–60]) who underwent three sequential MRIs (pre-, interim-, and post-NAC) and surgery were included. Patients' age, menopausal status, NAC regimens, and surgery details were obtained from their medical records.

MRI Protocol

Patients completed the three MRI scans at the following time points: 1) after diagnosis but before NAC (time point 0, TP0), 2) after NAC cycle 3 or 4 (time point 1, TP1), and 3) upon completion of NAC (cycle 6 or 8) but before surgery (time point 2, TP2). Breast MRIs were conducted using a 3-T system (Achieva, Philips Healthcare, Amsterdam, Netherlands) with the patients in a prone position with a dedicated breast coil (SENSE BREAST 7 Coil, Philips Healthcare). Prior to injection of a contrast medium, bilateral axial fat-suppressed T2-weighted images (repetition time/echo time, 5521 ms/70 ms; matrix, 332 × 261; field of view, 32 cm; flip angle, 90°; slice thickness, 3 mm with no gap; acquisition time, 4 min 23 s) were obtained. One pre-contrast and six post-contrast dynamic T1-weighted series were obtained at 55.4 s (axial), 110.8 s (axial), 146 s (sagittal), 221.6 s (axial), 292 s (sagittal), and 438 s (axial). Pre-contrast and post-contrast T1-weighted axial images were obtained using the following imaging parameters: repetition time/echo time, 4.42 ms/2.17 ms; matrix, 320 × 320; field of view, 32 cm; flip angle, 12°; slice thickness, 1 mm. The breast containing the cancer was supplementally scanned in the sagittal plane (repetition time/echo time, 4.37 ms/2.15 ms; matrix, 250 × 250; field of view, 25 cm; flip angle, 12°; slice thickness, 1 mm). Gadovist (Bayer Schering Pharma AG, Berlin, Germany) was injected by an automatic injector at a dose of 0.1 mmol/kg, at a rate of 2 mL/s, followed by a 25-mL saline flush. Standard subtraction images were created from the unenhanced and early and late contrast-enhanced fast low-angle shot (FLASH) sequences. Multiplanar reconstruction with coronal and sagittal scans and maximum-intensity-projection reconstructed images were also obtained.

CAD System

To measure MRI kinetic parameters, pre-contrast and all post-contrast T1-weighted images were transmitted to a commercially available CAD (CADstream; Confirma Inc., Kirkland, WA, USA). Three-dimensional tumor segmentation was con-

ducted automatically by CAD, which then calculated the tumor diameter (maximal size of an enhancing lesion), angiovolume (total enhancing lesion volume), peak enhancement (highest pixel signal intensity at the first post-contrast series), and delayed enhancement (proportions of persistent, plateau, and washout-enhancing components within a tumor) profiles. We selected an enhancement increment-threshold of 50% to compare the pre- and first post-contrast series, to increase sensitivity in the detection of slowly enhancing lesions commonly found in the NAC setting [10,11]. For each type of delayed phase enhancement after peak enhancement, a color map was set as follows: persistent type (indicating an increased pixel signal intensity of more than 10% from the first post-contrast series [blue color]); washout type (indicating a decreased pixel signal intensity at the last post-contrast series more than 10% from the first post-contrast series [red color]); and plateau type (demonstrating a change in either direction by less than 10% [green color]).

MRI Interpretation and Data Analysis

Two radiologists (E.S.C. and I.H.C.) with 26 and 3 years of breast MRI experience, respectively, were blinded to the pathological results and reviewed all the MRI scans in consensus. Tumor size was defined as the longest of the three-dimensional diameters and was measured at the 2nd phase of post-contrast T1 weighted image in all of the pre-, interim-, and post-NAC MRIs. Particularly, the tumor morphology (mass or mass with nonmass enhancement, nonmass enhancement) and multifocality were recorded in pre-NAC MRI. CAD-generated kinetic profiles were recorded as the proportion (%) of each total enhancement of the lesions allocated to persistent, plateau, and washout enhancement types. The percentage change of MRI parameters between pre-NAC and interim-NAC MRIs (ΔMRI value1), and between pre-NAC and post-NAC MRIs (ΔMRI value2) were calculated as follows:

$$\Delta\text{MRI value1} = \frac{\text{MRI value 1} - \text{MRI value 0}}{\text{MRI value 0}} \times 100,$$

$$\Delta\text{MRI value2} = \frac{\text{MRI value 2} - \text{MRI value 0}}{\text{MRI value 0}} \times 100,$$

where MRI value 0, MRI value 1, and MRI value 2 represent TP0 (pre-NAC), TP1 (interim-NAC), and TP2 (post-NAC) values, respectively. ΔMRI values included Δtumor size, Δpeak enhancement, Δpersistent, Δplateau, and Δwashout. If there was no color overlay at the location of the initial malignant lesion, the MRI value of persistent, plateau, and washout components were set as zero for calculating the percentage change.

Histopathologic Assessment

Pathologic data including pathologic tumor size, axillary nodal status, and breast cancer subtype by immunohistochemical (IHC) staining were obtained from the surgical pathology reports. RCB classes were retrospectively reviewed by one pathologist (S.H.S., with 24 years of experience in breast pathology). In this study, pCR was defined as the absence of invasive components in the primary tumor site (carcinoma in-situ may be present) based on the Miller and Payne classification, regardless of axillary nodal status [12]. RCB classes were categorized into one of four classes: RCB-0 (no RD), RCB-I (minimal RD), RCB-II (moderate RD), and RCB-III (extensive RD) based on the primary tumor diameter, cellularity of the tumor beds, and axillary lymph node burdens [3,13]. The expression status of estrogen receptor (ER), progesterone receptor (PR), and human epidermal growth factor receptor 2 (HER2) were evaluated in core biopsy specimens obtained at the time of diagnosis. ER or PR positivity was defined as at least 1% positive tumor nuclei in the sample by a 10× magnification field. The intensity of HER2 expression was initially scored as 0, 1+, 2+, or 3+ with IHC staining. Tumors with a score of 3+ were classified as HER2 positive, and tumors with scores of 0 or 1+ were classified as HER2 negative. When tumors showed an equivocal score (2+), a gene amplification with fluorescence-in-situ hybridization or silver-in-situ hybridization was performed to determine HER2 status. Breast cancer subtypes were classified according to their IHC staining, as follows: HR-positive/HER2-negative, HER2-positive, and triple-negative (HR- and HER2-negative).

Statistical Analysis

The clinical, pathological, and MRI parameters of breast cancer (including percentage changes in tumor diameter, peak enhancement, and proportions of persistent, plateau, and washout enhancing components) were compared between pCR and non-pCR patients. Categorical variables were analyzed using independent samples t-tests or Fisher's exact tests, and continuous variables were assessed using Kolmogorov-Smirnov (for normality) and Wilcoxon rank-sum tests. To differentiate pCR from non-pCR patients, receiver operator characteristics (ROCs) were calculated to determine the percentage change cut-offs for MRI parameters, followed by areas under the curve (AUC). To compare the percentage changes in MRI parameters of the four RCB classes, Kruskal-Willis tests and post-hoc pairwise comparisons using a Bonferroni correction were performed. Moreover, MRI parameters were compared between pCR and non-pCR patients for each breast cancer subtype using Wilcoxon rank-sum tests. p values less than 0.05 were regarded statistically significant. All statistical analyses were performed using SAS software (SAS, version 9.2, SAS Inc.; Cary,

NC, USA).

RESULTS

Patient Characteristics and Pathologic Response

The patients' characteristics according to pathologic response are summarized in Table 1. All the breast cancer cases (n = 51) were identified as invasive ductal carcinomas. Twenty-three (45.1%) tumors were HR positive/HER2 negative, 18 (35.3%) were HER2 positive, and 10 (19.6%) were triple negative. The median number of NAC cycles was 6 (range, 5–10). Thirty-six (70.6%) patients were treated with a taxane plus anthracycline–based regimen and 15 (29.4%) patients were treated with a taxane, anthracycline plus trastuzumab–based regimen.

pCR was achieved in 10/51 (19.6%) cases. Of the 10 pCR cases, 5 (50%) were HER2 positive, 3 (30%) were triple negative, and 2 (20%) were HR positive/HER2 negative. Upon final pathologic examination, 6 (11.8%) tumors were categorized as RCB 0, 7 (13.7%) as RCB I, 18 (35.3%) as RCB II, and 20 (39.2%) as RCB III. Mean age, menopausal status, axillary nodal status after NAC, breast cancer subtype, clinical staging, and type of surgery were not significantly different between the two groups.

Changes in MRI Parameters According to Pathologic Response

The MRI parameters according to pathologic response are summarized in Table 2. The Δtumor size2 (-96.9% vs. -41.1%, $p < 0.01$), Δpeak enhancement2 (-100% vs. -60.5%, $p = 0.01$), Δpersistent2 (-100% vs. 40.8%, $p = 0.01$), Δplateau2 (-100% vs. -50%, $p = 0.02$), and Δwashout2 (-100% vs. -90%, $p = 0.03$)

Table 1. Patient Characteristics According to Pathologic Response

Variable	All Patients (n = 51)	pCR* (n = 10)	Non-pCR* (n = 41)	p-Value
Age (yr), median (range)	48 (33–60)	50 (33–58)	47 (34–60)	0.27
Pathologic tumor size (mm)†, mean ± SD (median)	19.1 ± 25.7 (12)	0 (0)	23.8 ± 26.7 (15)	<0.01
Menopause status				0.30
Premenopausal	33 (64.7)	5 (50.0)	28 (68.3)	
Postmenopausal	18 (35.3)	5 (50.0)	13 (31.7)	
Axillary status (yp)				0.14
Negative	18 (35.3)	6 (60.0)	12 (29.3)	
Positive	33 (64.7)	4 (40.0)	29 (70.7)	
Histologic subtype				
IDC	51 (100)	10 (19.6)	41 (80.4)	NA
Tumor subtype				0.18
HR positive/HER2 negative	23 (45.1)	2 (20.0)	21 (51.2)	
HER2 positive	18 (35.3)	5 (50.0)	13 (31.7)	
Triple negative	10 (19.6)	3 (30.0)	7 (17.1)	
NAC regimen				>0.99
Taxane plus anthracycline	36 (70.6)	7 (70.0)	29 (70.7)	
Taxane, anthracycline plus trastuzumab	15 (29.4)	3 (30.0)	12 (29.3)	
Clinical TNM staging				>0.99
II	10 (19.6)	1 (10.0)	9 (22.0)	
III	36 (70.6)	9 (90.0)	27 (65.9)	
IV	5 (9.8)	0 (0)	5 (12.2)	
Type of surgery				0.49
Conserving surgery	24 (47.1)	6 (60.0)	18 (43.9)	
Mastectomy	27 (52.9)	4 (40.0)	23 (56.1)	
RCB class‡				<0.01
0	6 (11.8)	6 (60.0)	0 (0)	
I	7 (13.7)	2 (20.0)	5 (12.2)	
II	18 (35.3)	2 (20.0)	16 (39.0)	
III	20 (39.2)	0 (0.0)	20 (48.8)	

Data are numbers of patients (percentages) unless otherwise stated. *pCR was defined based on the Miller and Payne classification; †Pathologic tumor size was measured on surgical specimens; ‡RCB classes were calculated from the primary tumor dimensions, cellularity of the tumor beds, and axillary nodal burdens. pCR, pathologic complete response; IDC, invasive ductal carcinoma; HER2, human epidermal growth factor receptor 2; HR, hormone receptor; NAC, neoadjuvant chemotherapy; RCB, residual cancer burden

Table 2. MRI Parameters According to Pathologic Response

Variable	pCR* (n = 10)	Non-pCR* (n = 41)	p-Value
Tumor size, mean ± SD (median)			
Pre-NAC tumor size (mm)†	46 ± 19.7 (50.5)	60 ± 26.1 (56.6)	0.12
Interim-NAC tumor size (mm)†	30.5 ± 21.9 (29.9)	44.5 ± 25.3 (39.1)	0.12
Post-NAC tumor size (mm)†	9.9 ± 16.4 (0.5)	34.7 ± 23.5 (30.9)	<0.01
Morphology, n (%)			>0.99
Mass or mass with NME	8 (80)	31 (75.6)	
NME	2 (20)	10 (24.4)	
Multifocality, n (%)			0.16
No	7 (70)	17 (41.5)	
Yes	3 (30)	24 (58.5)	
ΔTumor size1 (%)	-34.8 (-77.9 to -12.7)	-20.1 (-100 to 34.8)	0.13
ΔTumor size2 (%)	-96.9 (-100 to -29)	-41.1 (-100 to -27.7)	<0.01
ΔPeak enhancement1 (%)	-55.7 (-81.1 to 85.5)	-61.2 (-98.2 to 58.7)	0.56
ΔPeak enhancement2 (%)	-100 (-100 to -47.3)	-60.5 (-100 to 78.3)	0.01
ΔPersistent1 (%)	37.8 (-44.2 to 1150)	64.6 (-78.1 to 18900)	0.32
ΔPersistent2 (%)	-100 (-100 to 1150)	40.8 (-100 to 21566.7)	0.01
ΔPlateau1 (%)	-64.4 (-100 to 200)	-56.5 (-100 to 271.4)	0.58
ΔPlateau2 (%)	-100 (-100 to 94.7)	-50 (-100 to 255.6)	0.02
ΔWashout1 (%)	-95.7 (-100 to 233.3)	-83.3 (-100 to 666.7)	0.24
ΔWashout2 (%)	-100 (-100 to 87.9)	-90 (-100 to 1000)	0.03

Data are medians (ranges) unless otherwise noted. *pCR was defined based on the Miller and Payne classification; †Pre-, interim-, post-NAC tumor size was measured using MRI. NAC, neoadjuvant chemotherapy; NME, nonmass enhancement; pCR, pathologic complete response

between the pCR and non-pCR patients, were significantly different (Figs. 1 and 2). However, there was no significant difference in the interim changes (Δtumor size1, Δpeak enhancement1, Δpersistent1, Δplateau1, and Δwashout1) between the two groups.

Table 3 shows the AUC with 95% confidence interval (CI), cut-off values, sensitivities, and specificities of percentage changes in MRI parameters that were associated with pCR. ΔTumor size2 (cut-off value, -90.0%; AUC, 0.88; 95% CI, 0.75–1.00) showed very good diagnostic accuracy. Additionally, Δpeak enhancement2 (cut-off value, -100%; AUC, 0.77; 95% CI, 0.59–0.95), Δpersistent2 (cut-off value, -95.8%; AUC, 0.78; 95% CI, 0.58–0.98), Δplateau2 (cut-off value, -100%; AUC, 0.74; 95% CI, 0.57–0.91), and Δwashout2 (cut-off value, -93.3%; AUC, 0.72; 95% CI, 0.56–0.88) showed good diagnostic accuracy. Interim changes in these parameters showed relatively poor diagnostic accuracy for pCR. ΔTumor size1 (cut-off value, -26.1%; AUC, 0.66; 95% CI, 0.46–0.86), Δwashout1 (cut-off value, -91.7%; AUC, 0.62; 95% CI, 0.42–0.83), Δpersistent1 (cut-off value, 87.5%; AUC, 0.60; 95% CI, 0.41–0.80) showed sufficient diagnostic accuracy. ΔPeak enhancement1 (cut-off value, -69.6%; AUC, 0.56; 95% CI, 0.38–0.75) showed bad diagnostic accuracy and Δplateau1 (cut-off value, 13.0%; AUC, 0.44; 95% CI, 0.20–0.68) was not a useful diagnostic factor.

Changes in Kinetic Profiles According to RCB Classes

There were significant difference in Δtumor size2 ($p < 0.01$), Δpeak enhancement2 ($p < 0.01$), Δplateau2 ($p < 0.01$), and Δwashout2 ($p < 0.01$) among the four groups (Table 4). The results of multiple post-hoc comparisons using a Bonferroni correction are presented in Figure 3. Multiple post-hoc comparisons with a Bonferroni correction revealed statistically significant differences ($p < 0.0083$) in Δtumor size2 between RCB-0 and RCB-II ($p = 0.0043$); RCB-0 and RCB-III ($p = 0.0003$); RCB-I and RCB-III ($p = 0.0012$); and RCB-II and RCB-III ($p = 0.0075$). Statistically significant differences were also found in Δpeak enhancement2 between RCB-I and RCB-III ($p = 0.0037$), Δplateau2 between RCB-I and RCB-III ($p = 0.0002$), and RCB-II and RCB-III ($p = 0.0012$), and Δwashout2 between RCB-I and RCB-III ($p = 0.0074$).

Changes in Kinetic Profiles According to Breast Cancer Subtype

The sequential percentage changes in MRI parameters by breast cancer subtype are summarized in Tables 5-7. In the triple negative group, there were significant differences in Δtumor size2 ($p < 0.01$), Δpersistent2 ($p < 0.01$), and Δplateau2 ($p = 0.01$) between pCR and non-pCR patients (Table 5). However, Δwashout2 did not differ significantly between the two groups ($p = 0.12$).

In the HR positive/HER2 negative (Table 6) and HER2 posi-

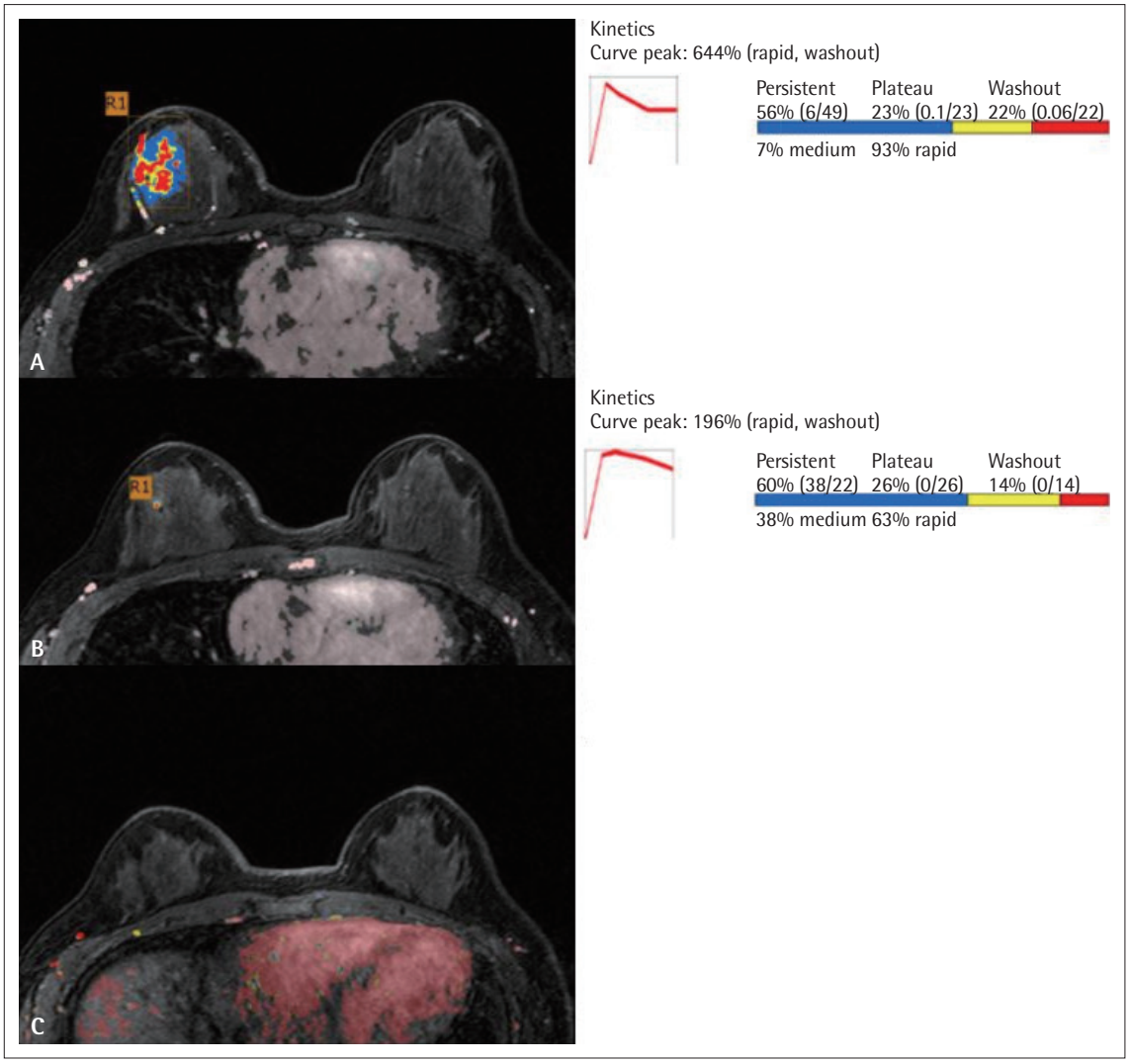

Fig. 1. MR CAD images of a 43-year-old woman with invasive ductal carcinoma (hormone receptor positive/human epidermal growth factor receptors type 2 negative). A: Pre-NAC MRIs. B: Interim-NAC MRIs. C: Post-NAC MRI. After NAC, the presumed malignant enhancing mass in the right breast markedly decreased without enhancement or CAD color map. There was no residual invasive carcinoma at final pathology (pathologic complete response). CAD, computer-aided detection; NAC, neoadjuvant chemotherapy.

tive types (Table 7), there were no significant differences in both interim and final changes in tumor size, and CAD-generated kinetic profiles between patients with pCR and with non-pCR, except for Δpeak enhancement2 in the HR positive/HER2 negative type (-100% vs. -71.7%, $p < 0.01$).

DISCUSSION

In our study, the final percentage changes in tumor size and CAD-generated kinetic profiles between pre-NAC and post-NAC MRIs showed significant differences between patients with pCR and with non-pCR. Also, the final percentage changes in tumor size, peak enhancement, plateau, and washout components differed according to the RCB classes. However, the interim percentage changes in tumor size and CAD-generated kinetic profiles between pre-NAC and interim-NAC MRIs were not associated with pCR.

NAC offers the opportunity to attain pCR, which is usually defined as the absence of residual invasive disease in the breast after NAC (pT0 or pTis), though the definition varies between clinical trials. The Miller and Payne grading system is based on the response of the primary tumor site only and ignores the tumor size and axillary nodal disease altogether [12]. However, the RCB classification developed at MD Anderson Cancer Centre overcomes these drawbacks, taking into account primary tumor dimension, tumor cellularity, and axillary nodal burden [13,14]. RCB was used as an accurate way to evaluate

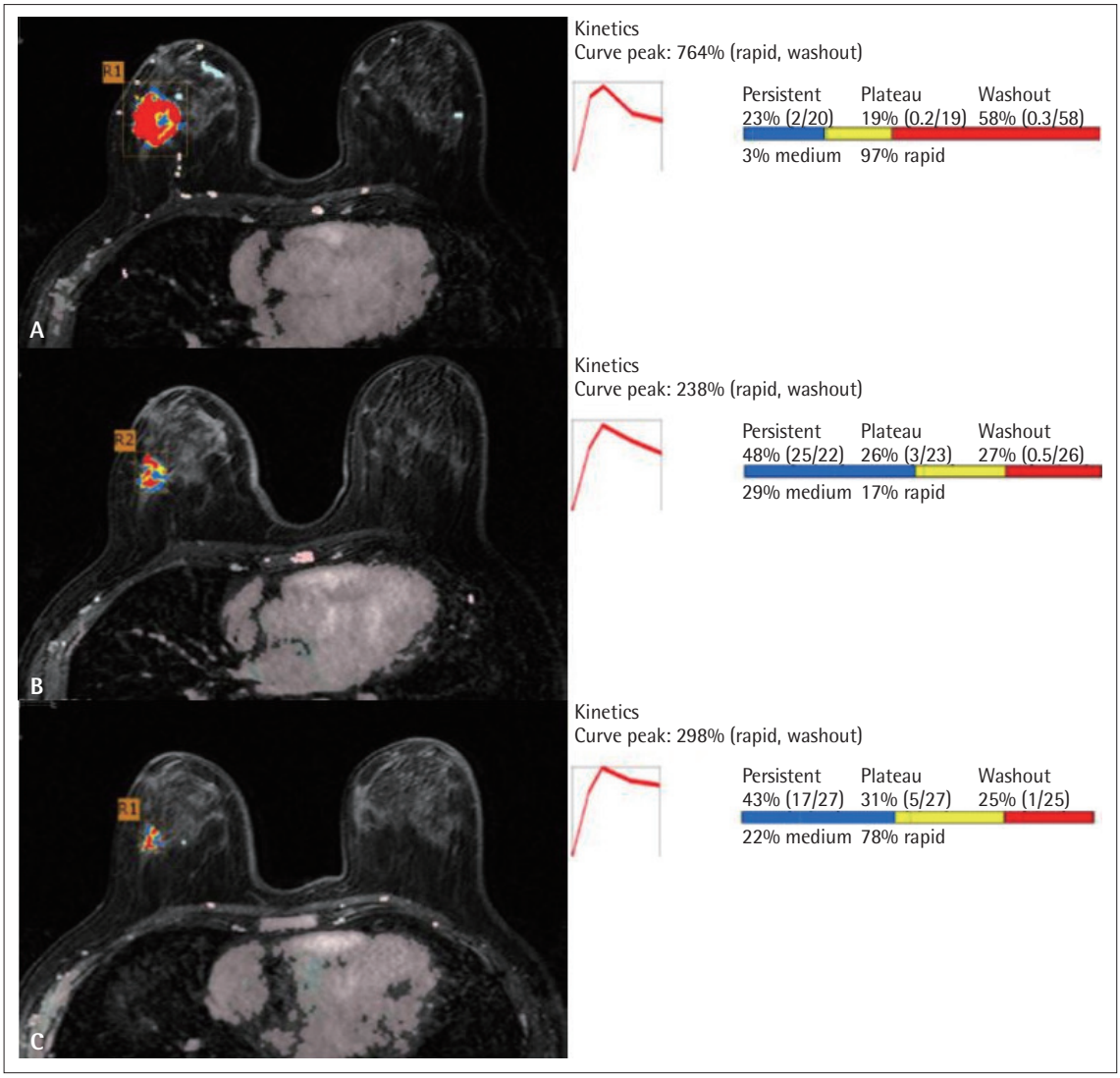

Fig. 2. MR CAD images of a 51-year-old woman with invasive ductal carcinoma (human epidermal growth factor receptors type 2 positive). A: Pre-NAC MRIs. B: Interim-NAC MRIs. C: Post-NAC MRIs. After completion of NAC, the persistent component increased by 87%, the plateau component increased by 63.2%, and the washout component decreased by 56.9% compared to the pre-NAC MRI. There was a 2.4-cm residual invasive carcinoma at final pathology, and the RCB class was III. CAD, computer-aided detection; NAC, neoadjuvant chemotherapy; RCB, residual cancer burden.

Table 3. Receiver Operating Characteristic Analysis for Pathologic Complete Response Prediction

Variable	AUC (95% CI)	Cut-Off Value (%)	Sensitivity	Specificity
ΔTumor size1	0.66 (0.46, 0.86)	-26.1	0.7	0.68
ΔPeak enhancement1	0.56 (0.38, 0.75)	-69.6	0.9	0.34
ΔPersistent1	0.60 (0.41, 0.80)	87.5	0.8	0.49
ΔPlateau1	0.44 (0.20, 0.68)	13.0	0.3	0.83
ΔWashout1	0.62 (0.42, 0.83)	-91.7	0.7	0.59
ΔTumor size2	0.88 (0.75, 1.00)	-90.0	0.7	0.95
ΔPeak enhancement2	0.77 (0.59, 0.95)	-100	0.6	0.93
ΔPersistent2	0.78 (0.58, 0.98)	-95.8	0.7	0.90
ΔPlateau2	0.74 (0.57, 0.91)	-100	0.8	0.71
ΔWashout2	0.72 (0.56, 0.88)	-93.3	0.9	0.54

AUC, area under the curve; CI, confidence interval

Table 4. MRI Parameters According to RCB Classes

Variable	RCB 0 (n = 6)	RCB I (n = 7)	RCB II (n = 18)	RCB III (n = 20)	p-Value
ΔTumor size1 (%)	-34.8 (-73.9 to -13.7)	-35 (-100 to -14.9)	-18.7 (-95.7 to 34.8)	-19.1 (-62.3 to 15.7)	0.05
ΔPeak enhancement1 (%)	-53.8 (-67.5 to 85.5)	-69.6 (-91.1 to -39.2)	-57.2 (-84.8 to -2.8)	-57.7 (-98.2 to 58.7)	0.46
ΔPersistent1 (%)	37.8 (-44.2 to 1150)	49.2 (0 to 165.7)	83.5 (-78.1 to 426.3)	69.5 (-76.3 to 18900)	0.87
ΔPlateau1 (%)	-64.4 (-100 to 200)	-88.5 (-100 to 13)	-69.3 (-100 to 64.7)	-39.3 (-93.9 to 271.4)	0.07
ΔWashout1 (%)	-95.7 (-100 to -40)	-89.5 (-100 to 0)	-95.1 (-100 to 327.3)	-69.3 (-98.9 to 666.7)	0.07
ΔTumor size2 (%)	-100 (-100 to -69.4)	-80.5 (-93.3 to -24.3)	-54.1 (-100 to 27.7)	-25.5 (-64.3 to 16.6)	<0.01
ΔPeak enhancement2 (%)	-100 (-100 to -47.3)	-93.2 (-100 to -60.5)	-62.2 (-100 to 78.3)	-51.8 (-98.4 to 48.5)	<0.01
ΔPersistent2 (%)	-100 (-100 to 1150)	53.8 (-100 to 112.8)	35.7 (-100 to 326.3)	24.2 (-74 to 21566.7)	0.10
ΔPlateau2 (%)	-100 (-100 to 94.7)	-100 (-100 to -100)	-84.1 (-100 to 42.3)	-16.5 (-100 to 255.6)	<0.01
ΔWashout2 (%)	-100 (-100 to 87.9)	-100 (-100 to 0)	-99.5 (-100 to 214.3)	-65.5 (-100 to 1000)	<0.01

Data are medians (ranges). RCB, residual cancer burden

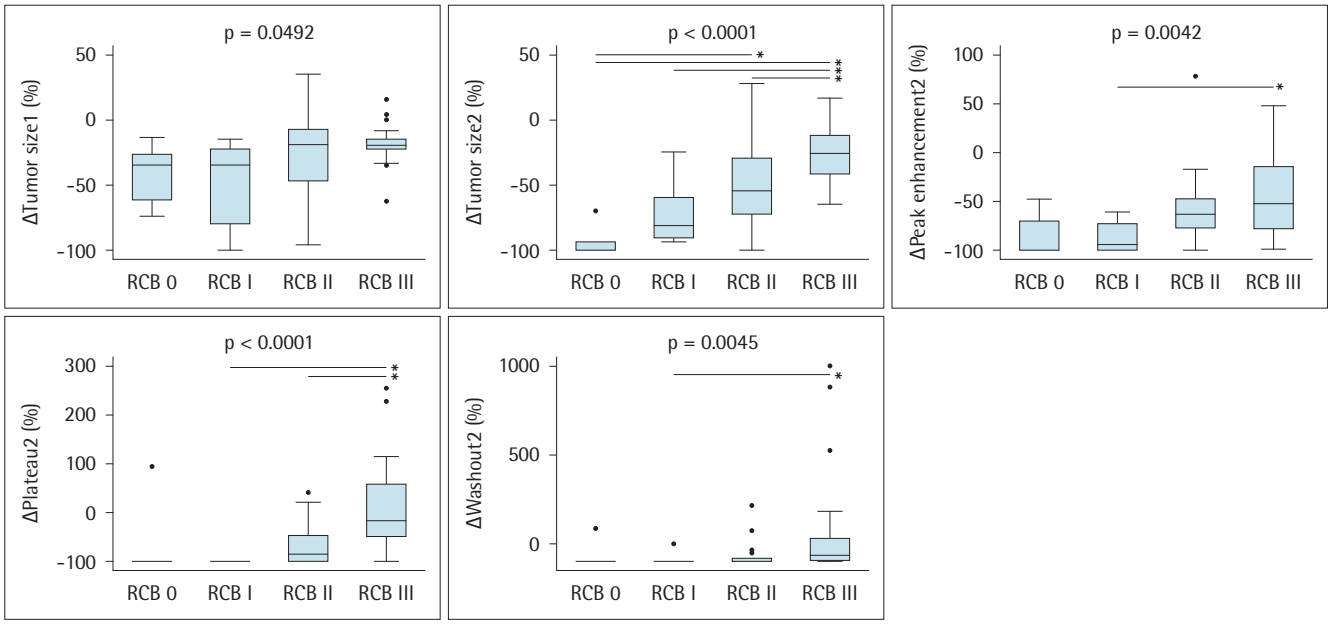

Fig. 3. Percentage changes in CAD generated kinetic profiles during NAC for four RCB classes. Δtumor size1 (p = 0.05), Δtumor size2 (p < 0.01), Δpeak enhancement2 (p < 0.01), Δplateau2 (p < 0.01), and Δwashout2 (p < 0.01) showed statistically significant differences among the RCB classes in the Kruskal-Willis test. *p < 0.0083; Bonferroni's post-hoc analysis. CAD, computer-aided detection; NAC, neoadjuvant chemotherapy; RCB, residual cancer burden.

Table 5. MRI Parameters in Triple-Negative Type Breast Cancer

Variable	Total (n = 10)	pCR (n = 3)	Non-pCR (n = 7)	p-Value
ΔTumor size1 (%)	-42.3 (-95.7 to -19.4)	-61.8 (-68.4 to -35.4)	-21.5 (-95.7 to -19.4)	0.59
ΔPeak enhancement1 (%)	-54.6 (-84.8 to 21)	-56.5 (-675 to -52.8)	-47.8 (-84.8 to 21)	0.47
ΔPersistent1 (%)	71.3 (-78.1 to 286.4)	38.5 (37.1 to 108.3)	104.1 (-78.1 to 286.4)	0.78
ΔPlateau1 (%)	-65.5 (-100 to 50)	-65.2 (-100 to -63.6)	-65.8 (-100 to 50)	0.41
ΔWashout1 (%)	-96 (-100 to 387.5)	-97.4 (-100 to -91.7)	-95 (-100 to 387.5)	0.51
ΔTumor size2 (%)	-56.2 (-100 to 16.6)	-100 (-100 to -100)	-41.2 (-72.6 to 16.6)	<0.01
ΔPeak enhancement2 (%)	-77.1 (-100 to 78.3)	-100 (-100 to -100)	-47 (-82.2 to 78.3)	0.05
ΔPersistent2 (%)	23.8 (-100 to 163.9)	-100 (-100 to -100)	56.3 (-45.3 to 163.9)	<0.01
ΔPlateau2 (%)	-78.6 (-100 to 7.7)	-100 (-100 to -100)	-47.4 (-100 to 7.7)	0.01
ΔWashout2 (%)	-99.7 (-100 to 525)	-100 (-100 to -100)	-90 (-100 to 525)	0.12

Data are medians (ranges). pCR, pathologic complete response

Table 6. MRI Parameters in HR Positive/HER2 Negative Type Breast Cancer

Variable	Total (n = 23)	pCR (n = 2)	Non-pCR (n = 21)	p-Value
ΔTumor size1 (%)	-17.9 (-100 to 9.1)	-56 (-77.9 to -34.2)	-17.7 (-100 to 9.1)	0.15
ΔPeak enhancement1 (%)	-64.6 (-98.2 to 85.5)	8 (-69.6 to 85.5)	-64.6 (-98.2 to 58.7)	0.31
ΔPersistent1 (%)	100 (-76.3 to 18900)	5.1 (3.1 to 7.1)	100 (-76.3 to 18900)	0.13
ΔPlateau1 (%)	-56.5 (-100 to -271.4)	-43.5 (-100 to 13)	-56.5 (-100 to 271.4)	0.71
ΔWashout1 (%)	-91.7 (-100 to 666.7)	-68.2 (-100 to -36.4)	-91.7 (-100 to 666.7)	>0.99
ΔTumor size2 (%)	-30.7 (-100 to -1.1)	-95 (-100 to -90)	-30 (-100 to -1.1)	0.06
ΔPeak enhancement2 (%)	-72.9 (-100 to -48.5)	-100 (-100 to -100)	-71.7 (-100 to 48.5)	<0.01
ΔPersistent2 (%)	69.4 (-100 to 21566.7)	-100 (-100 to -100)	77.1 (-100 to 21566.7)	0.06
ΔPlateau2 (%)	-67.6 (-100 to 255.6)	-100 (-100 to -100)	-56.3 (-100 to 255.6)	0.10
ΔWashout2 (%)	-94.9 (-100 to 1000)	-100 (-100 to -100)	-94.9 (-100 to 1000)	0.17

Data are medians (ranges). HER2, human epidermal growth factor receptor 2; HR, hormone receptor; pCR, pathologic complete response

Table 7. MRI Parameters in HER2 Positive Type Breast Cancer

Variable	Total (n = 18)	pCR (n = 5)	Non-pCR (n = 13)	p-Value
ΔTumor size1 (%)	-21.2 (-73.9 to 34.8)	-14.9 (-73.9 to -12.7)	-22.2 (-62.3 to 34.8)	0.92
ΔPeak enhancement1 (%)	-54 (-81.1 to -16.4)	-54.9 (-81.1 to -16.4)	-53.2 (-75.9 to -21.2)	>0.99
ΔPersistent1 (%)	37 (-47.3 to 1150)	53.8 (-44.2 to 1150)	35.9 (-47.3 to 252.9)	0.85
ΔPlateau1 (%)	-49.8 (-100 to 200)	-52.6 (-100 to 200)	-47.1 (-100 to 36.8)	>0.99
ΔWashout1 (%)	-65 (-100 to 333.3)	-93.9 (-100 to 233.3)	-60 (-100 to 333.3)	0.39
ΔTumor size2 (%)	-554 (-100 to 27.7)	-69.4 (-100 to -29)	-46.8 (-85.1 to 27.7)	0.16
ΔPeak enhancement2 (%)	-58.4 (-100 to 3.3)	-69.4 (-100 to -47.3)	-57.4 (-100 to 3.3)	0.50
ΔPersistent2 (%)	13.3 (-100 to 1150)	13.8 (-100 to 1150)	13 (-100 to 87)	0.92
ΔPlateau2 (%)	-73.5 (-100 to 94.7)	-100 (-100 to 94.7)	-42.9 (-100 to 63.2)	0.68
ΔWashout2 (%)	-82.4 (-100 to 883.3)	-100 (-100 to 87.9)	-56.9 (-100 to 883.3)	0.34

Data are medians (ranges). HER2, human epidermal growth factor receptor 2; pCR, pathologic complete response

the extent of RD after NAC and is a strong prognostic predictor [3]. Compared to pCR which has already been heavily studied, studies which evaluate the association between RCB with radiologic features are relatively rare.

In our study, pCR was achieved in 10/51 (19.6%) tumors. We found that triple-negative (30%) and HER2 positive (27.8%) tumors had better responses to NAC than HR positive/HER2 negative tumors (8.7%). These results are consistent with those of previous studies [2,15-17], and may be explained by high rates of cellular proliferation in these breast cancer subtypes. This makes them more susceptible to chemo-agent induced apoptosis and cell necrosis. Also, trastuzumab target therapy is very effective in HER2 positive tumors [18].

Now that NAC is more commonly used, response assessment to NAC as well as precise prediction of pCR before surgery has emerged as an important issue. DCE-MRI outperforms conventional methods, such as physical examination, mammography, and sonography [19]. The major advantage of DCE-MRI over the conventional imaging methods is that it is a functional modality that can assess treatment-induced changes in tumor cellularity and vasculature. In our study, the decrease in the washout component of tumors after NAC in the non-pCR group (Δwashout2 = -90%) was lower compared to the pCR group (Δwashout2 = -100%). Likewise, the decrease in the washout component of tumors after NAC in the RCB III group (Δwashout2 = -65.5%) was lower compared to the RCB 0, I, and II groups (Δwashout2 = -100%, -100%, and -99.5%, relatively). Yi et al. [9] reported that a smaller reduction in the washout component of tumors using DCE-MRI after NAC was predictive of lower rates of recurrence-free survival and overall survival. They proposed that the residual washout component after NAC was indicative of chemotherapy-resistant cancer cells, leading to a worse survival outcome. In our study, we found that patients with non-pCR (Δplateau2 = -50%) had significantly less reduction in the plateau component compared to patients with pCR (Δplateau2 = -100%) at the final change. In a previous study by Kim et al. [6] using DCE-MRI with CAD, a higher pre-treatment plateau component within a tumor was significantly correlated with non-pCR. They assumed that it might be due to tumor angiogenesis. Similarly, we inferred that the residual plateau component might have been associated with the residual tumor vascular burden after NAC. Interestingly, patients with non-pCR (Δpersistent2 = 40.8%) showed a significant increase in the persistent compo-

nent compared to patients with pCR (Δpersistent2 = -100%) at the final change. Persistent enhancement patterns are usually associated with benignity or fibrosis [6,20]. Although chemotherapy-induced fibrosis may occur more often in pCR than non-pCR, the persistent component in patients with non-pCR paradoxically increased relative to pCR. We attributed this to a reduction in tumor size and a loss of tumor enhancement. Therefore, a significant increase in the persistent component of non-pCR compared to pCR reflects the therapeutic response for both pCR and non-pCR.

Similarly, the final changes in tumor size ($p < 0.01$) and CAD generated kinetic profiles between pCR and non-pCR were also significant in the triple-negative subtype (Δpersistent2; $p < 0.01$, Δplateau2; $p = 0.01$). Previous studies have reported that the diagnostic accuracy of MRI varies by breast cancer subtype in the NAC setting; HR negative/HER2 positive and triple negative types show higher accuracy than HR positive/HER2 negative types [15-17]. In our study, HER2 positive and HR positive/HER2 negative types did not show significant final changes in tumor diameter or kinetic profiles between pCR and non-pCR patients.

RCB classes are significant predictors of distant relapse-free survival in breast cancer patients undergoing NAC [3]. Symmans et al. [3] found that patients with RCB-I showed the same 5-year prognosis as those with RCB-0 and patients with RCB-III showed a poor prognosis. They suggested that the combination of RCB-0 and RCB-I expanded the subset of patients who profited from NAC. We found that final changes in tumor diameter, plateau, and washout components were associated with RCB classes ($p < 0.01$). There was a statistically significant difference in Δtumor size2 between RCB-0 and RCB-II ($p = 0.0043$) and between RCB-0 and RCB-III ($p = 0.0003$). There were statistically significant differences in Δtumor size2 ($p = 0.0012$), Δpeak enhancement2 ($p = 0.0037$), Δplateau2 ($p = 0.0002$), and Δwashout2 ($p = 0.0074$) between RCB-I and RCB III. There were statistically significant differences in Δtumor size2 ($p = 0.0075$) and Δplateau2 ($p = 0.0012$) between RCB-II and RCB-III. Our results showed no statistically significant differences in MRI parameters between RCB-0 and RCB-I and between RCB-I and RCB-II.

Our study had some limitations. First, it was a retrospective study with a relatively small sample size from a single institution. Therefore, we hope to validate our results with a larger cohort in the future. Second, due to the short follow-up interval after surgery, we were unable to identify if the percentage changes in kinetic profiles during NAC were associated with recurrence-free or overall survival outcomes. Third, we evaluated the association between RCB classes and primary tumor response only without considering radiologic axillary nodal responses.

In conclusion, the results of this study indicate that MRI using CAD shows is a potential means of predicting pCR and RCB classes. However, the early prediction of pathologic response to NAC using MRI with CAD is still limited.

Availability of Data and Material

The datasets generated or analyzed during the study are available from the corresponding author on reasonable request.

Conflicts of Interest

The authors have no potential conflicts of interest to disclose.

Author Contributions

Conceptualization: In Hye Chae, Eun-Suk Cha. Data curation: In Hye Chae, Eun-Suk Cha, Jee Eun Lee, Jin Chung, Jeoung Hyun Kim, Sun Hee Sung. Formal analysis: Mira Han. Investigation: In Hye Chae, Eun-Suk Cha. Methodology: In Hye Chae, Eun-Suk Cha, Mira Han. Supervision: Eun-Suk Cha. Writing—original draft: In Hye Chae. Writing—review & editing: In Hye Chae, Eun-Suk Cha. Approval of final manuscript: all authors.

ORCID iDs

In Hye Chae https://orcid.org/0000-0001-6093-1761
Eun-Suk Cha https://orcid.org/0000-0001-9588-2074
Jee Eun Lee https://orcid.org/0000-0003-4451-7661
Jin Chung https://orcid.org/0000-0001-9990-3768
Jeoung Hyun Kim https://orcid.org/0000-0003-3504-9595
Sun Hee Sung https://orcid.org/0000-0001-9345-1131
Mira Han https://orcid.org/0000-0002-3557-7710

Funding Statement

None

REFERENCES

1. von Minckwitz G, Untch M, Blohmer JU, et al. Definition and impact of pathologic complete response on prognosis after neoadjuvant chemotherapy in various intrinsic breast cancer subtypes. J Clin Oncol 2012;30:1796-1804.
2. Houssami N, Macaskill P, von Minckwitz G, Marinovich ML, Mamounas E. Meta-analysis of the association of breast cancer subtype and pathologic complete response to neoadjuvant chemotherapy. Eur J Cancer 2012;48:3342-3354.
3. Symmans WF, Peintinger F, Hatzis C, et al. Measurement of residual breast cancer burden to predict survival after neoadjuvant chemotherapy. J Clin Oncol 2007;25:4414-4422.
4. Rauch GM, Adrada BE, Kuerer HM, van la Parra RF, Leung JW, Yang WT. Multimodality imaging for evaluating response to neoadjuvant chemotherapy in breast cancer. AJR Am J Roentgenol 2017;208:290-299.
5. Marinovich ML, Houssami N, Macaskill P, et al. Meta-analysis of magnetic resonance imaging in detecting residual breast cancer

after neoadjuvant therapy. J Natl Cancer Inst 2013;105:321-333.
6. Kim H, Kim HH, Park JS, et al. Prediction of pathological complete response of breast cancer patients undergoing neoadjuvant chemotherapy: usefulness of breast MRI computer-aided detection. Br J Radiol 2014;87:20140142.
7. Böttcher J, Renz DM, Zahm DM, et al. Response to neoadjuvant treatment of invasive ductal breast carcinomas including outcome evaluation: MRI analysis by an automatic CAD system in comparison to visual evaluation. Acta Oncol 2014;53:759-768.
8. Demartini WB, Lehman CD, Peacock S, Russell MT. Computer-aided detection applied to breast MRI: assessment of CAD-generated enhancement and tumor sizes in breast cancers before and after neoadjuvant chemotherapy. Acad Radiol 2005;12:806-814.
9. Yi A, Cho N, Im SA, et al. Survival outcomes of breast cancer patients who receive neoadjuvant chemotherapy: association with dynamic contrast-enhanced MR imaging with computer-aided evaluation. Radiology 2013;268:662-672.
10. Partridge SC, Gibbs JE, Lu Y, et al. MRI measurements of breast tumor volume predict response to neoadjuvant chemotherapy and recurrence-free survival. AJR Am J Roentgenol 2005;184:1774-1781.
11. Williams TC, DeMartini WB, Partridge SC, Peacock S, Lehman CD. Breast MR imaging: computer-aided evaluation program for discriminating benign from malignant lesions. Radiology 2007;244:94-103.
12. Ogston KN, Miller ID, Payne S, et al. A new histological grading system to assess response of breast cancers to primary chemotherapy: prognostic significance and survival. Breast 2003;12:320-327.
13. Residual Cancer Burden Calculator. The University of Texas, MD Anderson Cancer Center. Available from: https://www.mdanderson.org/breastcancer_RCB. Accessed April 1, 2022.
14. Fumagalli D, Bedard PL, Nahleh Z, et al. A common language in neoadjuvant breast cancer clinical trials: proposals for standard definitions and endpoints. Lancet Oncol 2012;13:e240-e248.
15. Loo CE, Straver ME, Rodenhuis S, et al. Magnetic resonance imaging response monitoring of breast cancer during neoadjuvant chemotherapy: relevance of breast cancer subtype. J Clin Oncol 2011;29:660-666.
16. van la Parra RF, Kuerer HM. Selective elimination of breast cancer surgery in exceptional responders: historical perspective and current trials. Breast Cancer Res 2016;18:28.
17. Chen JH, Bahri S, Mehta RS, et al. Breast cancer: evaluation of response to neoadjuvant chemotherapy with 3.0-T MR imaging. Radiology 2011;261:735-743.
18. Goldhirsch A, Wood WC, Coates AS, Gelber RD, Thürlimann B, Senn HJ. Strategies for subtypes--dealing with the diversity of breast cancer: highlights of the St. Gallen International Expert Consensus on the Primary Therapy of Early Breast Cancer 2011. Ann Oncol 2011;22:1736-1747.
19. Yeh E, Slanetz P, Kopans DB, et al. Prospective comparison of mammography, sonography, and MRI in patients undergoing neoadjuvant chemotherapy for palpable breast cancer. AJR Am J Roentgenol 2005;184:868-877.
20. Macura KJ, Ouwerkerk R, Jacobs MA, Bluemke DA. Patterns of enhancement on breast MR images: interpretation and imaging pitfalls. Radiographics 2006;26:1719-1734; quiz 1719.